Astron. Astrophys. 360, 663–670 (2000)

ASTRONOMY AND ASTROPHYSICS

Tracing the root of the bipolar jet in IRAS 20126+4104: VLBA observations of H_2O masers⋆

L. Moscadelli[1], **R. Cesaroni**[2], **and M.J. Rioja**[3]

[1] Stazione Astronomica di Cagliari, Loc. Poggio dei Pini, strada 54, 09012 Capoterra (Cagliari), Italy
[2] Osservatorio Astrofisico di Arcetri, Largo E. Fermi 5, 50125 Firenze, Italy
[3] Observatorio Astronomico Nacional (IGN), Apartado 1143, 28800 Alcalá de Henares (Madrid), Spain

Received 21 December 1999 / Accepted 26 April 2000

Abstract. We present VLBA observations of the H_2O masers towards IRAS 20126+4104, a high-mass young stellar object which is believed to be associated with a rotating disk and a bipolar outflow/jet system collimated along the disk axis. A model fit to the positions and velocities of the maser spots demonstrates that these could arise on a conical surface at the interface between the jet and the surrounding molecular gas. The masers expand from a common centre which coincides, within the uncertainties, with the position of the embedded young stellar object: the expansion velocity is less than that measured on a much larger scale in the SiO(2–1) line and this indicates that the jet is sensitively braked close to its origin by the interaction with the surrounding medium.

Key words: masers – ISM: individual objects: IRAS 20126+4104 – ISM: jets and outflows – radio lines: ISM

1. Introduction

The study of the environment where star formation is going on has been made possible by observations of molecular lines which permit a derivation of the physical parameters of the region. The temperature and density of the gas can be obtained from the ratio of the intensities of different transitions of the same molecule. Although such techniques can be applied to almost all molecular species and lines, they fail with the "masing" transitions, namely those originating from pairs of levels with inverted populations. The maser photons undergo a process of exponential amplification by stimulated emission which makes it difficult to relate the resulting line intensity to the physical parameters of the emitting gas. However, an important exception to this rule is represented by the velocity field: since the maser amplification mechanism requires good velocity coherence along the line of sight, the narrow masing lines represent excellent tracers of the corresponding component of the gas velocity.

This characteristic has been successfully used by many authors to study the kinematics of various environments, especially well ordered velocity fields such as those present in disks, jets, outflows, or expanding shells. It is worth stressing that high angular resolution ($\ll 1''$) is necessary to identify and locate the compact spots from which the maser line arises. The best known example is probably represented by the OH line maps, which nicely identify the approaching and receding portions of the expanding circumstellar shells around OH/IR stars (see e.g. Cohen 1989). Another striking application is represented by the VLBI observations of the H_2O masers in the active galaxy NGC 4258 (Miyoshi et al. 1995), which trace a Keplerian rotating disk around a massive black hole at the centre of the galactic nucleus. In the context of star formation, similar examples are represented by the CH_3OH masers in NGC 7538 (Minier et al. 1998) and SiO masers in Orion IRc2 (Baudry et al. 1998), which also appear to trace a rotating disk. However, H_2O masers in star forming regions seem to be associated both with rotating and expanding motions, namely with disks and outflows (Chernin 1995; Fiebig et al. 1996; Torrelles et al. 1997; Torrelles et al. 1998). The association between outflows and H_2O masers is also suggested by theoretical models such as that of Elitzur et al. (1989), where the inversion occurs in shocks at the interface between the ejected material and the surrounding molecular gas. Models for H_2O masers tracing rotating disks have been also proposed by some authors (e.g. Cesaroni 1990; Fiebig 1997).

With this in mind, we have performed high angular resolution observations towards the H_2O maser associated with the high-mass young stellar object (YSO) IRAS 20126+4104. This source is interesting because it is probably the best studied and simplest example of a massive (proto)star (with luminosity $\sim 10^4\ L_\odot$) associated with a Keplerian disk and a jet/outflow system. The latter is directed along the axis of the disk. The molecular outflow has been mapped by Cesaroni et al. (1997) and Shepherd et al. (1999) on a scale $\geq 20''$. Observations at millimeter and centimeter wavelengths have shown that the outflow is fed by a jet, which can be progressively traced down to $\sim 1''$ through line emission of H_2 (Cesaroni et al. 1997), SiO(2–1) (Cesaroni et al. 1999, hereafter C99), CO(7–6) (Kawamura et al.

Send offprint requests to: L. Moscadelli (mosca@ca.astro.it)

⋆ Based on observations carried out with the Very Large Baseline Array. The VLBA is a facility of the NRAO, which is operated by Associated Universities, Inc., under contract with the NSF.

1999), NH_3(3,3) (Zhang et al. 1999), and continuum emission at 3.6 cm (Hofner et al. 1999). On the other hand, CH_3CN(5–4) observations (Cesaroni et al. 1997) have revealed a molecular disk almost perpendicular to the jet axis and rotating around the embedded YSO at the origin of the outflow/jet. Subsequent observations in the CH_3CN(12–11) (C99) and NH_3(1,1) lines (Zhang et al. 1998b) have found evidence for Keplerian rotation, implying a stellar mass of $\sim$24 $M_\odot$.

Notwithstanding the large amount of data, information on angular scales $\ll 1''$ is scarce, being represented only by the Very Large Array (VLA) observations of Tofani et al. (1995; hereafter TFTH). These authors observed the water maser line at 22.2 GHz with an angular resolution of $0\farcs1$ and identified three centers of emission: two displaced to the NW and SE of the YSO and probably associated with the jet, and a third closer to the disk. Each centre emits more than one spectral feature (see Fig. 14 of TFTH) and should hence be resolved into many spots with higher angular resolution, such as that attainable with very long baseline radio interferometry ($\sim$1 mas). At the distance of IRAS 20126+4104 (1.7 kpc) this corresponds to a linear size of $\sim$1.7 AU, which is obviously of great interest for studying circumstellar disks and planet formation and for investigating the mechanism powering the jets. On the basis of the results of TFTH, we decided to perform VLBA observations of the H_2O masers in IRAS 20126+4104 with the goal of assessing the structure and kinematics of the gas associated with the disk *and* the jet.

Technical details of the observations are given in Sect. 2 and the results are illustrated in Sect. 3, where a comparison with other data is also made. The interpretation is discussed in Sect. 4, while the conclusions are drawn in Sect. 5.

2. Observations and data reduction

IRAS 20126+4104 was observed with the NRAO Very Long Baseline Array (VLBA) on November 21 and 22, 1997, for a total of 12 hours at 22 GHz. The tracking of the source was periodically interrupted, every hour, by a 6.5 minutes of observation of one of the continuum calibrator sources, 1803+784 or 3C454.3.

The stations recorded an aggregate of 8 MHz bandwidth in both circular polarisations, centered at the LSR velocity of –3.5 km s^{-1} (based upon a rest frequency of 22235.0798 MHz), using 2-bits sample (mode 64–2–2). The correlation was made at the VLBA correlator in Socorro (New Mexico) using 512 spectral channels uniformly weighted, which gives a full width half maximum (FWHM) velocity resolution of 0.18 km s^{-1} and a channel separation of 0.21 km s^{-1}.

The calibration of the observed visibilities and the mapping were accomplished with the NRAO AIPS package. We used the system temperatures ($T_{\rm sys}$) and the antenna gain information provided in the VLBA calibration tables for the amplitude calibration of both the calibrators and the program source. The measured $T_{\rm sys}$ for all antennas was in a range between 85 and 110K, except for St. Croix and Handcock, with an average of 150K. The gain factors for all VLBA antennas at 22 GHz range from 0.07 K Jy^{-1} to 0.013 K Jy^{-1}. The insufficient signal-to-noise ratio (SNR) of the total power spectra of the program source prevented using the "template spectrum" method (which consists of comparing spectra of different scans) to estimate corrections to the nominal amplitude gain factors.

The scans on the calibrators are used to complete the calibration of the observed phases for the program source. First, the instrumental single-band delay and the phase offset between the two polarisations were derived by fringe-fitting a single scan of the strong continuum source 3C454.3. Then, after removing the instrumental errors, all calibrator scans were fringe-fitted to determine the residual (time-dependent) delay and the fringe rate. The phase corrections derived from calibrators were applied to the IRAS 20126+4104 data. A reference maser channel was chosen with good SNR and a simple structure for self-calibration. Plots of visibility amplitude versus baseline length suggested that the most suitable channel was at 13.6 km s^{-1} (containing the peak flux density). This channel was found to contain two maser spots (#22 and #23 in Table 1) separated by $\sim$2.4 mas. The visibilities in this channel were fringe fitted to find the residual fringe rate produced by differences in atmospheric fluctuations affecting the calibrators and the target, and errors in the nominal source coordinates used at the correlator. The corrections derived from the phase and the rate self-calibration of the reference channel were applied to all channels of the maser data.

Using the AIPS task "IMAGR", $2\farcs5\times1\farcs25$ (E$\times$N) naturally weighted maps centered on the reference feature were produced for all channels in the velocity range from –27 km s^{-1}to +16 km s^{-1}, which includes all the features apparent in the total power spectra. The restoring (CLEAN) beam was an elliptical gaussian with half power width (HPBW) of 1.2$\times$1.1 mas oriented at a position angle of 49°. The 1σ RMS noise level on the channel maps, calculated using an area where no signal is found, is 4–5 mJy beam^{-1} for all the channels.

Every channel map was searched for emission above a certain threshold and the detected emission features were fitted with single or multiple gaussians, determining position, integrated and peak flux, and full width at half power (FWHP) of the spots. The threshold used was the absolute value of the minimum in the map, which varies from channel to channel in the range 20–50 mJy beam^{-1}. A feature was considered real if it was found in at least two contiguous spectral channels at the same position, within an uncertainty equal to the FWHP obtained with the gaussian fit. The errors on the positions (given in Table 1) have been calculated with the relation $\Delta\theta = 0.5\,{\rm HPBW/SNR}\,\sqrt{N/2}$ (Richards et al. 1999), where SNR is the ratio between the peak intensity and the 1σ noise in the corresponding spectral channel, and $N = 10$ is the number of antennae used.

By comparing the residual fringe rates of the maser reference feature and the calibrators, the offset of the reference maser feature from the position used by the correlator was derived. The absolute position of the reference feature is α(J2000)=$20^{\rm h}\,14^{\rm m}\,26\fs0387$, δ(J2000)=41° 13′ 32$\farcs$534 with an uncertainty of 30 mas.

Table 1. Parameters of the water maser spots. The offsets are given with respect to spot #23. The spot position and the full width half power (non deconvolved) have been obtained with a 2-D gaussian fit. Numbers in parentheses represent positional uncertainties calculated as explained in the text

#	V_{LSR} (km s^{-1})	$F_{\rm int}$ (Jy)	$F_{\rm peak}$ (Jy beam^{-1})	$\Delta\alpha$ (mas)	$\Delta\delta$ (mas)	Maj.Ax. (mas)	Min.Ax. (mas)
1	–24.2	0.26	0.07	–101.988(0.074)	108.945(0.073)	3.1	1.6
2	–22.7	0.06	0.06	–120.151(0.089)	128.597(0.088)	1.3	1.1
3	–22.9	0.22	0.05	–123.803(0.108)	124.979(0.107)	4.0	1.5
4	–23.9	0.10	0.05	–106.580(0.100)	121.263(0.098)	2.2	1.2
5	–20.8	0.07	0.07	–119.546(0.080)	118.050(0.079)	1.4	1.1
6	–20.8	0.27	0.05	–123.174(0.100)	114.120(0.098)	3.9	1.8
7	–24.2	0.13	0.11	–98.472(0.049)	112.842(0.048)	1.4	1.2
8	–8.2	0.10	0.10	–110.587(0.054)	154.394(0.053)	1.2	1.1
9	–7.1	0.09	0.04	–107.905(0.144)	153.097(0.142)	1.6	1.5
10	–7.9	1.45	0.96	–106.919(0.005)	152.008(0.005)	1.6	1.2
11	–9.4	0.21	0.18	–108.613(0.029)	151.513(0.028)	1.3	1.2
12	–7.3	3.50	3.41	–105.754(0.002)	150.957(0.002)	1.2	1.1
13	–11.9	0.26	0.20	–110.888(0.026)	150.620(0.026)	1.4	1.2
14	–12.6	0.12	0.10	–110.100(0.052)	149.133(0.051)	1.4	1.1
15	–5.6	0.03	0.03	–117.195(0.192)	89.645(0.190)	1.2	1.0
16	–5.8	0.04	0.03	–114.216(0.152)	84.560(0.150)	1.6	1.0
17	–6.5	0.65	0.60	–120.844(0.009)	67.216(0.009)	1.2	1.1
18	–7.3	0.35	0.35	–116.158(0.022)	64.235(0.022)	1.2	1.1
19	–11.9	0.06	0.04	–151.256(0.118)	61.285(0.116)	1.5	1.1
20	2.4	0.08	0.08	–117.841(0.062)	61.200(0.062)	1.3	1.1
21	11.0	0.17	0.12	0.026(0.044)	2.540(0.043)	1.5	1.2
22	13.6	1.90	1.87	–0.457(0.003)	2.380(0.003)	1.2	1.1
23	13.6	3.08	2.75	0.000	0.000	1.4	1.1
24	12.3	0.53	0.53	0.904(0.010)	–0.030(0.010)	1.2	1.1
25	–3.3	0.29	0.25	–794.285(0.020)	342.709(0.020)	1.2	1.2
26	–3.3	0.15	0.05	–797.650(0.096)	338.476(0.095)	2.6	1.4

3. Results

A total of 26 H_2O maser spots were detected towards IRAS 20126+4104. The parameters listed in Table 1 are those of the fit (see Sect. 2) performed in the channel where the spot intensity is maximum. Note that in some cases the FWHP is greater than the HPBW: we believe that this is due to overlap of two or more distinct spots having similar velocities and positions. In any case, the SNR is too poor to allow any definite conclusion about resolving the structure of single spots. Fig. 1 illustrates the distribution of the H_2O maser spots with respect to other tracers from previous observations. In the top panel we plot the jet seen in the 3.6 cm continuum (contours), the CH_3CN(12–11) peaks tracing the disk (filled circles), the H_2O masers mapped by TFTH with the VLA (triangles), and the peak position (yellow cross) and the size (yellow circle) of the 1.3 mm continuum emission. The bottom panels show enlargements of the regions where H_2O maser emission was detected in the VLBA observations.

It is important to stress that, while the absolute position of the H_2O masers measured with the VLBA is known with great accuracy ($\sim$30 mas; see Sect. 2), that of the other tracers is much more uncertain. In particular, the position of the CH_3CN and 1.3 mm continuum peaks has a 1σ error of $\sim 0\farcs3$. Therefore, in the following we shall assume an uncertainty of $0\farcs9$ on the position of the disk – and hence of the YSO – with respect to the H_2O maser spots.

The most evident result is the lack of maser emission towards the spot seen by TFTH to the SE (named C3 by them), although the corresponding velocity interval is properly covered by our frequency set-up and the area mapped ($2\farcs5$ in right ascension and $1\farcs25$ in declination) is much wider than that over which the three spots of TFTH are spread. This cannot be explained by missing flux in our VLBA maps, as one can see in Fig. 2, where the integrated flux density of the synthesised channel maps is compared to a single dish spectrum acquired with the Medicina 32-m antenna[1] two days before the VLBA observations. Clearly, the two spectra are perfectly coincident within the noise and we recover all the single-dish flux in our VLBA maps. In addition to the masers in C3 and to those towards the centre of the map (spot C2 in the notation of TFTH), TFTH detected emission also from a region to the NW (spot C1 in their notation): although no emission is seen in our maps at exactly the same position, we do detect a pair of spots roughly $0\farcs2$ to the W of C1.

The differences between our results and those of TFTH are not surprising. H_2O masers are well known to be highly variable even on periods as short as a few weeks, hence the long time

[1] The Medicina telescope is operated by the Istituto di Radioastronomia, C.N.R., Bologna

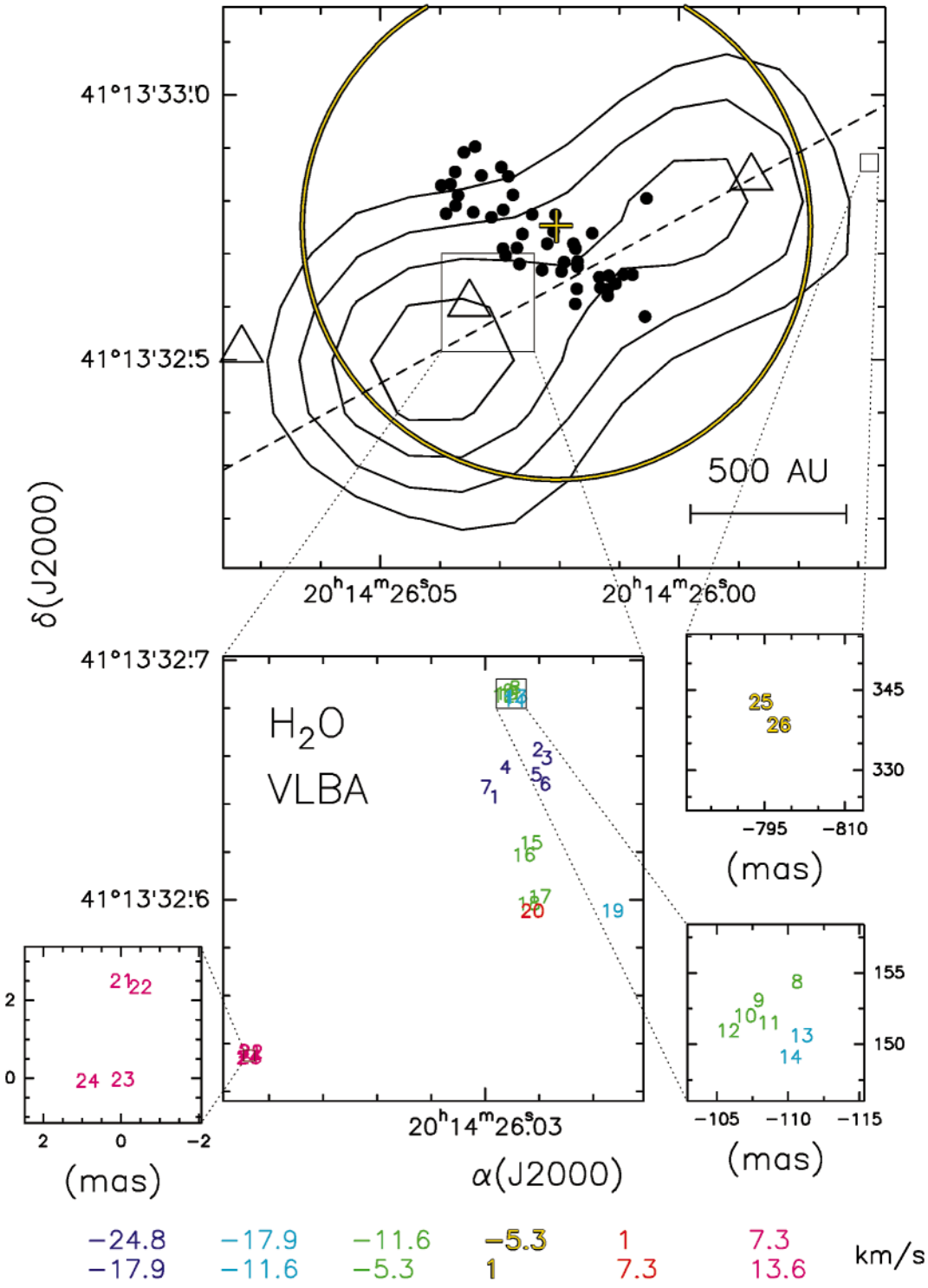

Fig. 1. *Top panel:* composite map of the 3.6 cm continuum emission (contours) from Hofner et al. (1999), $CH_3CN(12–11)$ (filled circles) and 1.3 mm continuum (yellow cross and circle) from C99, and H_2O maser spots (triangles) from TFTH: the cross and circle indicate the peak and diameter of the millimeter continuum emission according to Table 4 of C99. Contour levels are 0.03 to 0.11 by 0.02 mJy beam^{-1}. The dashed line represents the symmetry axis of the jet. Note that the angular resolution changes considerably from tracer to tracer, being $\sim$0.″7 for $CH_3CN(12–11)$ and the 1.3 mm continuum, $\sim$0.″5 for the 3.6 cm continuum, $\sim$0.″1 for the H_2O masers by TFTH. *Bottom panels:* enlargements of the regions outlined in the top panel, showing the distribution of the H_2O maser spots seen in the VLBA observations. Each spot is identified by the number listed in column 1 of Table 1, while the colour indicates the velocity of the spot, according to the coding shown at the bottom of the figure. Note that in the three smallest panels the coordinates given in the figures are offsets computed with respect to the position of spot #23

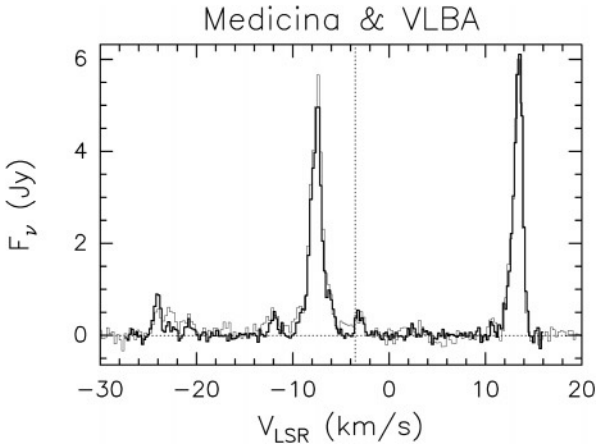

Fig. 2. Comparison between Medicina single dish spectrum (thin line) and integrated flux density (thick line) of the synthesised channel maps. The horizontal and vertical dotted lines indicate respectively the zero emission level and the systemic LSR velocity (–3.5 km s^{-1}) of the molecular clump associated with the masers

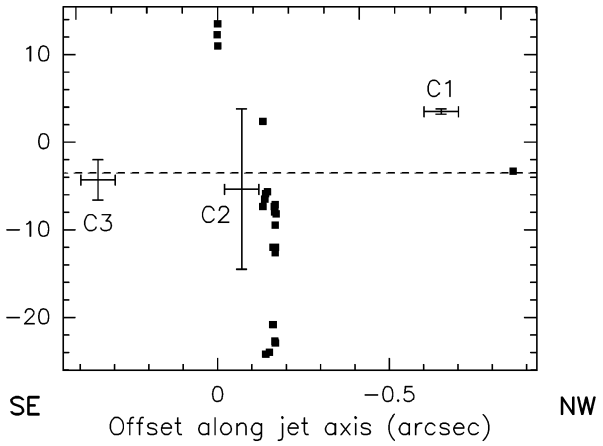

Fig. 3. The LSR velocities of the H_2O maser spots seen in the present VLBA observations (filled squares) and in the VLA map of TFTH (bars) are plotted against the corresponding offset along the direction of the jet axis (the dashed line in Fig. 1). The offset is computed with respect to the position of spot #23. The vertical bars indicate the velocity interval over which maser emission is detected, according to Table 2 of TFTH, and the horizontal ones represent the VLA HPBW. The dashed line corresponds to the systemic LSR velocity (–3.5 km s^{-1})

span ($\sim$7 years) between our observations and those of TFTH fully explains the observed changes. The masers in the central spot C2 seem much more persistent, although the corresponding spectrum has undergone a radical change (compare Fig. 2 with Fig. 14 of TFTH). A possible interpretation is that the H_2O masers in C2 are more easily triggered being closer to the central engine (the embedded YSO) than masers such as those in C1 and C3 which lie much further away.

It is also interesting to note that the velocities of spots C1 and C3 are significantly different from those observed in C2. As one can see in Fig. 3, C1 and C3 differ by less than ± 6 km s^{-1} from the systemic LSR velocity (~ -3.5 km s^{-1}) of the bulk material (i.e. the LSR velocity of the YSO), much less than the ± 20 km s^{-1} velocity dispersion observed towards C2. Two explanations are possible: (i) spots C1 and C3 are moving in directions almost perpendicular to the line of sight; or (ii) the motion of the spots is slowed down at large distances from the centre. The spots #25 and 26 detected in the VLBA observations are likely of the same nature as spot C1 and may hence be of great help to decide which of the two hypotheses is correct: indeed, in Sect. 4.1 we shall demonstrate that explanation (i) is to be preferred.

In conclusion, the spots in C1 and C3 seem related to the jet from the YSO. But what is the nature of the masers in C2? Are they related to the disk or to the jet? Given their proximity to the YSO both hypotheses are plausible. In the next section we present a model that represents a possible answer to these questions.

4. Interpretation and discussion

In the following model we use only the VLBA observations of H_2O masers, given their superior sensitivity and resolution. Also, one must remember that the location of the disk (i.e. of the CH_3CN peaks) with respect to the masers is of limited use, given the large uncertainty in its position (see Sect. 3).

By looking at the bottom panels of Fig. 1 a first consideration is in order. The velocities of the spots are not consistent with those expected in the rotating disk seen by C99: since the axis of the disk is parallel to that of the jet, if the masers were lying in the disk their velocities should be mostly blue shifted to the NE and red shifted to the SW, as in the case of CH_3CN (see Fig. 5c of C99), whereas no such trend is visible. Instead, the "reddest" and "bluest" spots lie respectively to the SE and NW, along a direction parallel to the jet axis. This situation is more similar to the jet model presented by C99: in fact, if the masers lie on the surface of a cone and move radially away from a common centre, one expects to see the maximum and minimum velocities along the direction of the cone axis, whereas the velocity should decrease down to the systemic value of –3.5 km s^{-1} moving away from the axis. This is in reasonable agreement with the trend in Fig. 1. In order to check if this hypothesis is consistent with the data, we have elaborated a simple jet model analogous to that presented by C99.

4.1. Jet model

We assume that the masers arise on the surface of a conical bipolar jet, at the interaction zone between the ionised jet and the surrounding neutral medium. The vertex of the cone coincides with the embedded YSO. The velocity of a spot is directed radially outward from the YSO and has a constant value, v_0, independent of the distance from the centre. We assume a coordinate system centred in the vertex of the cone, with z axis along the line of sight and x axis coincident with the projection of the jet axis on the plane of the sky (see Fig. 4). Under the assumption that the observer lies at $z = -\infty$, the component of the velocity along the line of sight is given by

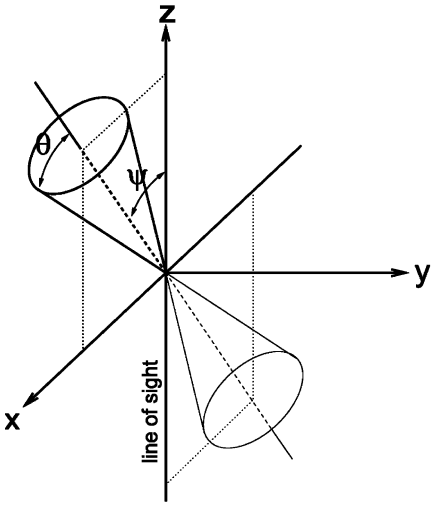

Fig. 4. Sketch of the conical jet model. The observer lies at $z = -\infty$, i.e. the plane of the sky coincides with plane x–y. The origin of the axes is the location of the YSO powering the jet. The x axis is the projection of the jet axis on the plane of the sky

$$v_z = v_0 \frac{z}{\sqrt{x^2+y^2+z^2}}. \quad (1)$$

Also, we indicate with ψ the inclination angle between the jet axis and the z axis, and with 2θ the opening angle of the cone (see Fig. 4). Since the spots lie on the surface of the cone, z must satisfy the condition

$$\begin{aligned} z \;=\; & \Big[x \sin\psi\cos\psi\,(1+\tan^2\theta) \\ & \pm \tan\theta \sqrt{x^2+y^2(\cos^2\psi - \tan^2\theta\sin^2\psi)} \Big] \times \\ & \times \left(\tan^2\theta\sin^2\psi - \cos^2\psi\right)^{-1}. \end{aligned} \quad (2)$$

In our model we know the direction of the jet axis in the plane of the sky (see Fig. 1), which has a position angle of 119°, but the position of the vertex of the cone is unknown and we indicate it with (α_0, δ_0).

We thus have a total of five free parameters, namely v_0, θ, ψ, α_0, and δ_0. A few constraints can be applied to these. By definition, $v_0 > 0$ and $0 < \theta < 90°$. Also, it makes sense to rule out apertures and inclinations of the cone that make it cross the line of sight, because we know that the lobes of the jet/outflow are well separated in the plane of the sky (see e.g. C99): this is equivalent to the condition $\theta < \psi < 180° - \theta$. Finally, the vertex of the cone is expected to coincide with the embedded YSO, and hence with the centre of the disk; as explained in Sect. 3, the absolute position of the CH_3CN disk has a probable error of 0.″9: we can thus assume that α_0 and δ_0 must lie within $\pm$0.″9 of the millimeter continuum peak, which can be taken as a good approximation of the YSO position.

Under these assumptions and for a given set of input parameters, one can compute v_z for each spot position and compare it with the observed velocity. Note that before making this comparison, the systemic velocity of –3.5 km s^{-1} must be added to the velocity obtained from Eq. (1). The best fit to the data was obtained in two steps. First, we found the values of θ, ψ, α_0, and δ_0 that minimise the expression

$$\chi^2 = \sum_{i=2}^{26} \left(\frac{v_z^{(i)}}{v_z^{(1)}} - \frac{V_z^{(i)}}{V_z^{(1)}} \right)^2 \quad (3)$$

where we have indicated with $v_z^{(i)}$ the velocity of spot #i calculated from Eqs. (1) and (2) and with $V_z^{(i)}$ the difference between the observed LSR velocity of the spot and the systemic LSR velocity –3.5 km s^{-1}; note that the expression for χ^2 has the advantage of being independent of v_0, thus reducing the number of free parameters to four. Then, we fixed θ, ψ, α_0, and δ_0 to the values derived above: in this way Eq. (1) becomes a linear expression in v_0, which is thus computed with a standard least square fit.

The best fit is obtained for $\psi = 59°$, $\theta = 29°$, $v_0 = 23$ km s^{-1}, α_0(J2000)=20^h 14^m 26.^{s}037, δ_0(J2000)=41° 13′ 32.″56 and is shown in Fig. 5. The top panel presents the projection of the conical jet on the plane of the sky and the position of the maser spots, while in the bottom panel we compare the observed velocities of the spots with those computed by the model. Clearly the agreement is very good, especially if one takes into account that local deviations of a few km s^{-1} from the velocity field are to be expected, due to turbulence at the interface between the jet and the surrounding medium. It is worth stressing the fact that even the most distant spots from the jet origin (#25 and 26 in Fig. 1) are well fitted by our model: this supports the assumption that the expansion velocity remains constant along the jet.

We conclude that our model is consistent with the data, but in order to prove the uniqueness of the interpretation more information is needed, such as, for example, proper motion measurements of the maser spots. These can be easily predicted by the model and should be equal to $\sim$3 mas yrs^{-1}, easy to observe with global VLBI.

4.2. Discussion

Given the goodness of the fit, a few considerations are in order. The parameters obtained are roughly consistent with those derived by C99 fitting the SiO emission of the jet, namely ψ=78°–87° and θ=9°–22°: clearly, the most significant discrepancy is that in ψ. However, a slight change in the inclination may be expected, given the large range of size scales involved, going from 10^3 AU (the size of the H_2O jet) to 2 10^4 AU (the size of the SiO jet). Precession of the jet axis might be an explanation: this hypothesis seems indeed supported by recent results obtained by Shepherd et al. (1999) who found evidence for precession in IRAS 20126+4104, by comparing the structure of the jet/outflow system on scales ranging from 0.1 pc to 1 pc.

On the other hand, the good agreement in θ is surprising, because it indicates that the collimation mechanism of the jet must remain very effective going from $\sim$50 AU (the minimum distance of the maser spots to the centre) to $\sim$0.1 pc (the scale size of the SiO emission).

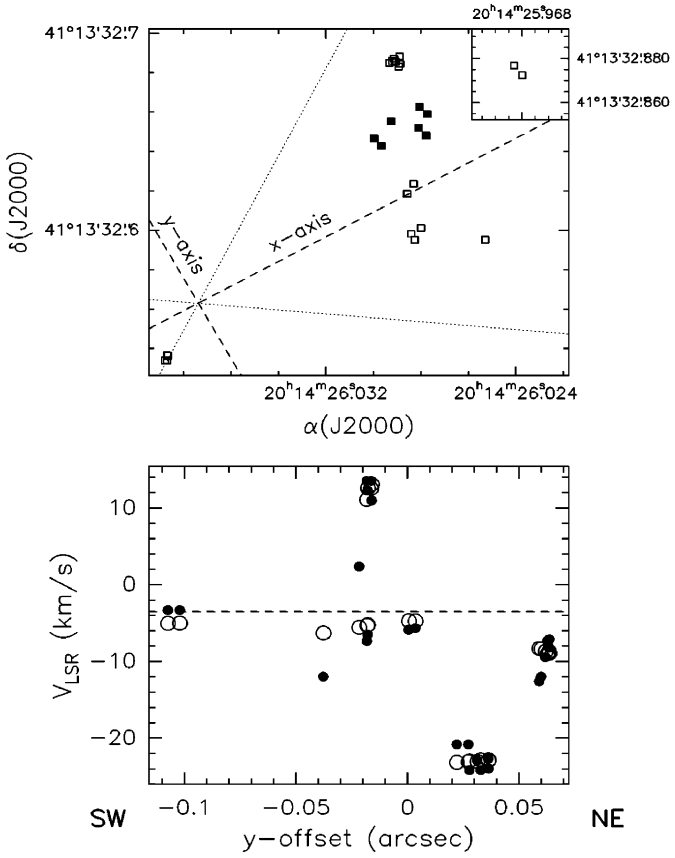

Fig. 5. *Top panel:* map of the H_2O maser spots and sketch of the projection on the plane of the sky of the best fit conical jet model. Filled squares represent maser spots lying on the surface of the cone facing the observer, whereas empty squares indicate spots on the rear side. The x-axis is the projection of the cone axis on the plane of the sky. The points in the inset correspond to spots #25 and 26 (see Fig. 1). *Bottom panel:* comparison between the spot LSR velocity observed (solid circles) and obtained from the model best fit (empty circles). The abscissa represents the offset perpendicular to the axis of the cone. The dashed line corresponds to the systemic LSR velocity of –3.5 km s^{-1}. Note that the two points with y-offset of –0.″1 correspond to the spots in the inset of the top panel

It is also worth noting that our model is consistent with the expansion velocity remaining constant at least on the region traced by the H_2O masers: this is indeed expected in the model of Stahler (1994), which describes the velocity structure of the material entrained by molecular outflows. Furthermore, the low value of 23 km s^{-1} found for the intrinsic velocity of the spots is consistent with the findings for the SiO jet. The results of C99 indicate that the velocity of the jet increases with distance from the centre up to values as high as $\gtrsim$100 km s^{-1}. The minimum SiO line width is measured towards the YSO and corresponds to $\sim$20 km s^{-1} once a correction for the inclination angle is applied: such a value well compares to v_0.

In conclusion, we believe that the H_2O masers in IRAS 20126+4104 arise in a dense neutral layer on the surface of an ionised conical jet. On a scale two orders of magnitude larger, the jet becomes neutral and is seen in molecular tracers such as SiO and H_2. The study of the SiO and H_2O line emission indicates that the jet is well collimated on scales ranging from 0.″1 to 10″ and gives important clues on its velocity field. The model fit to the H_2O maser spots presented above suggests that the velocity of the neutral material at the interface between the jet and the surrounding molecular gas could remain approximately constant as long as the jet digs its way through the dense molecular surroundings. On a larger scale, however, the velocity increases up to a (de-projected) value of $\sim$100 km s^{-1}. The most trivial interpretation is that the expansion is accelerated at a constant rate of $\sim$1200 km s^{-1} pc^{-1} (see the model fit to the SiO(2–1) line emission presented by C99) as soon as the jet breaks out of the core and is hence not braked anymore by the high-density molecular gas surrounding the YSO. However, if the SiO line emission arises from lower-density material entrained by the flow, such an acceleration could be explained by the outflow model of Stahler (1994), where the expansion velocity is constant along any given radial direction and only a transversal velocity gradient is required.

The existence of strong interaction between the ionised jet and the core is supported by the fact that the jet weakens dramatically beyond the core border. This is illustrated in the top panel of Fig. 1, where the extent of the millimeter continuum emission from the core is shown by the yellow circle, drawn according to the parameters given in Table 4 of C99: clearly, the 3.6 cm continuum emission is detected only inside the region delimited by the circle, namely where high density gas is present.

Finally, we want to verify that the momentum in the jet is sufficient to explain the H_2O maser emission. This is equivalent to check that the ratio between the mechanical luminosity of the jet ($L_{\rm w}$) and the mechanical luminosity of the shocks exciting the masers ($L_{\rm m\,H_2O}$) is $\sim$1. An estimate of $L_{\rm m\,H_2O}$ is obtained from Eq. (2) of Felli et al. (1992), who made use of the model by Elitzur et al. (1989), while $L_{\rm w}$ can be estimated by means of the expression given by TFTH and Eq. (24) of Panagia & Felli (1975) for the ratio between mass loss rate and expansion velocity of the wind. We can thus write the previous ratio as:

$$\begin{aligned}\frac{L_{\rm w}}{L_{\rm m\,H_2O}} \;=\; & 463\, S_\nu^{0.75}({\rm mJy})\, d^{1.5}({\rm kpc})\, \nu^{-0.45}({\rm GHz}) \\ & T^{-0.075}(10^4{\rm K})\, n_{\rm H_2}^{-1}(10^7{\rm cm^{-3}}) \\ & D^{-2}(10^{13}{\rm cm})\, N_{\rm spots}^{-1}\, a^{-4} \left(\frac{1}{1-\cos\theta}\right)^{0.75}\end{aligned} \qquad (4)$$

where S_ν is the continuum flux measured at frequency ν, d is the distance to the source, T the temperature of the ionised gas, $n_{\rm H_2}$ the density of the gas where at the masers form, $N_{\rm spots}$ the number of H_2O maser spots, D their diameter in the plane of the sky, and a the "aspect ratio", i.e. the ratio between the length of the maser spot along the line of sight and D. Note that the previous expression depends quite weakly on most parameters but very strongly on a, which ranges from $a = 1$ for spherical masers to $a \gg 1$ for filamentary masers. Note also that the factor $1/(1-\cos\theta)$ is a correction introduced to take into account that in our conical model the ionised gas is collimated into an angle

2θ, whereas Eq. (24) of Panagia & Felli (1975) is derived under the assumption of spherical symmetry.

The majority of the parameters in Eq. (4) are known from this work or previous studies, so that we can assign them the following values: $T = 10^4$ K, $S_\nu = 0.34$ mJy at $\nu = 8.4$ GHz (Hofner et al. 1999), $d = 1.7$ kpc, $n_{\rm H_2} = 10^8$ cm^{-3} (Cesaroni et al. 1997), $N_{\rm spots} = 26$, and $\theta = 29°$. Eventually one obtains

$$\frac{L_{\rm w}}{L_{\rm m\,H_2O}} \simeq \frac{3.2}{D^2(10^{13}{\rm cm})\,a^4}. \quad (5)$$

In principle D and a are unknown: in fact, the spots are not resolved by our observations and it is impossible to know the length of the masing region along the line of sight. However, high angular resolution VLBI studies in regions such as W49N (Gwinn 1994) have shown that $D = 10^{13}$ cm can be a reasonable guess for an H_2O maser spot. Therefore, Eq. (5) turns into $L_{\rm w}/L_{\rm m\,H_2O} \simeq 3.2/a^4$. We conclude that the two luminosity estimates are comparable *only if* $a \simeq 1$: as soon as a exceeds $3.2^{1/4} \simeq 1.3$ the previous ratio becomes $\ll$1.

This suggests that *if* masers arise from the interaction of an ionised jet with the surrounding molecular medium, then maser spots are likely to be spherical rather than filamentary.

5. Conclusions

We have performed VLBA observations of the H_2O maser line at 22235.07985 MHz towards the high-mass YSO IRAS 20126+4104. A total of 26 maser spots have been detected and their distribution has been compared with other tracers such as the CH_3CN(12–11) transition and the 1.3 mm and 3.6 cm continuum emission. IRAS 20126+4104 is a rare example of high-mass (proto)star in which evidence for a rotating disk and a bipolar flow ejected along the disk axis has been found: the goal of the observations was to assess whether the H_2O masers are related to the disk or to the jet and to use them as tracers to sample the velocity field on a scale of $\sim$100 AU.

We demonstrate that the velocities and the distribution of the spots can be adequately reproduced by a model where the spots lie on the surface of a conical bipolar jet and move radially from the vertex of the cone with constant velocity. The best fit is obtained by minimising the difference between the observed velocities and those computed from the model at the positions of the spots. The result demonstrates that the aperture and inclination of the cone are in reasonable agreement with those derived on the basis of previous SiO(2–1) observations of the jet. We interpret this as evidence for an efficient ejection and/or collimation mechanism which keeps the direction and beaming of the jet almost constant on scales ranging from $\sim$50 AU to $\sim$0.1 pc.

A further step to better understand the structure and evolution of the jet will be represented by observations of H_2O maser proper motions, which we expect to be of the order of $\sim$3 mas yrs^{-1} and hence measurable with VLBI techniques.

Acknowledgements. We would like to thank Malcolm Walmsley and Steve Stahler for critically reading the manuscript and for stimulating discussions. Jim Herrnstein and Lincoln Greenhill are kindly acknowledged for making available the software that we used to determine the astrometric positions. We also thank the referee, Anita Richards, for useful comments on the manuscript. This project was partially supported by ASI grant ARS-98-116 to the Osservatorio Astrofisico di Arcetri

References

Baudry A., Herpin F., Lucas R., 1998, A&A 335, 654
Cesaroni R., 1990, A&A 233, 513
Cesaroni R., Felli M., Testi L., Walmsley C.M., Olmi L., 1997, A&A 325, 725
Cesaroni R., Felli M., Jenness T., et al., 1999, A&A 345, 949 (C99)
Chernin L., 1995, ApJ 440, L97
Cohen R.J., 1989, Rep. Prog. Phys. 52, 881
Elitzur M., Hollenbach D.J., McKee C.F., 1989, ApJ 346, 983
Felli M., Palagi F., Tofani G., 1992, A&A 255, 293
Fiebig D., 1997, A&A 327, 758
Fiebig D., Duschl W.J., Menten K.M., Tscharnuter W.M., 1996, A&A 310, 199
Gwinn C.R., 1994, ApJ 429, 253
Hofner P., Cesaroni R., Rodríguez L.F., Martí J., 1999, A&A 345, L43
Kawamura J.H., Hunter T.R., Tong C.-Y.E., et al., 1999, PASP 111, 1088
Minier V., Booth R.S., Conway J.E., 1998, A&A 336, L5
Miyoshi M., Moran J., Herrnstein J., et al., 1995, Nat 373, 127
Panagia N., Felli M., 1975, A&A 39, 1
Richards A.M.S., Yates J.A., Cohen R.J., 1999, MNRAS 306, 954
Shepherd D.S., Yu K.C., Bally J., Testi L., 1999, ApJ in press
Stahler S.W., 1994, ApJ 422, 616
Tofani G., Felli M., Taylor G.B., Hunter T.R., 1995, A&AS 112, 299 (TFTH)
Torrelles J.M., Gomez J.F., Rodríguez L.F., et al., 1997, ApJ 489, 744
Torrelles J.M., Gomez J.F., Rodríguez L.F., et al., 1998, ApJ 505, 756
Zhang Q., Hunter T.R., Sridharan T.K., 1998b, ApJ 505, L151
Zhang Q., Hunter T.R., Sridharan T.K., Cesaroni R., 1999, ApJ 527, L117